



Article

Enhanced Peroxidase-Like Activity of MoS₂ Quantum Dots Functionalized g-C₃N₄ Nanosheets towards Colorimetric Detection of H₂O₂

Peng Ju ^{1,2}, Yunhong He ³, Min Wang ⁴, Xiuxun Han ⁵, Fenghua Jiang ², Chengjun Sun ^{2,6,*}  and Chi Wu ^{1,*}

¹ Institute of Marine Science and Technology, Shandong University, 72 Binhai Road, Qingdao 266237, China; jupeng@fio.org.cn

² Key Laboratory of Marine Bioactive Substances and Analytical Technology, Marine Ecology Center, The First Institute of Oceanography, State Oceanic Administration (SOA), 6 Xianxialing Road, Qingdao 266061, China; jiangfh@fio.org.cn

³ Key Laboratory of Marine Chemistry Theory and Technology, Ministry of Education, Ocean University of China, 238 Songling Road, Qingdao 266100, China; yunhong_he@163.com

⁴ Shandong Provincial Key Laboratory of Chemical Energy Storage and Novel Cell Technology, Liaocheng University, Liaocheng 252000, China; 13619349919@163.com

⁵ Institute of Semiconductor Materials, Jiangxi University of Science and Technology, 86 Hongqi Road, Ganzhou 341000, China; xxhan@licp.cas.cn

⁶ Laboratory of Marine Drugs and Bioproducts, Pilot National Laboratory for Marine Science and Technology (Qingdao), 1 Wenhai Road, Qingdao 266237, China

* Correspondence: csun@fio.org.cn (C.S.); qwcnsd@163.com (C.W.); Tel.: +86-532-88963310 (C.S.); +86-532-58633229 (C.W.)

Received: 5 November 2018; Accepted: 23 November 2018; Published: 26 November 2018



Abstract: MoS₂ quantum dots (QDs) functionalized g-C₃N₄ nanosheets (MoS₂@CNNS) were prepared through a protonation-assisted ion exchange method, which were developed as a highly efficient biomimetic catalyst. Structural analysis revealed that uniformly-dispersed MoS₂ QDs with controllable size and different loading amount grew in-situ on the surface of CNNS, forming close-contact MoS₂@CNNS nanostructures and exhibiting distinct surface properties. Compared to MoS₂ QDs and CNNS, the MoS₂@CNNS nanocomposites exhibited a more than four times stronger peroxidase-like catalytic activity, which could catalyze the oxidation of 3,3',5,5'-tetramethylbenzidine (TMB) in the presence of H₂O₂ to generate a blue oxide. Among the MoS₂@CNNS nanocomposites, MoS₂@CNNS(30) was verified to present the best intrinsic peroxidase-like performance, which could be attributed to the more negative potential and larger specific surface area. A simple, rapid and ultrasensitive system for colorimetric detection of H₂O₂ was thus successfully established based on MoS₂@CNNS, displaying nice selectivity, reusability, and stability. The detection limit of H₂O₂ could reach as low as 0.02 μM. Furthermore, the kinetic and active species trapping experiments indicated the peroxidase-like catalytic mechanism of MoS₂@CNNS. This work develops a novel, rapid, and ultrasensitive approach for visual assay of H₂O₂, which has a potential application prospect on clinical diagnosis and biomedical analysis.

Keywords: MoS₂; g-C₃N₄; peroxidase-like; colorimetric detection; H₂O₂

1. Introduction

Over past decades, enzyme mimetics have caused extensive concern due to their favorable superiorities against harsh conditions compared to natural enzymes, such as low cost, easy preparation

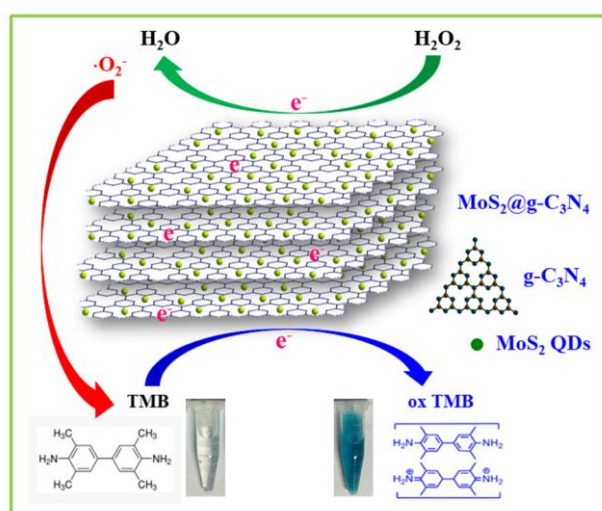
and storage, better stability and reusability, and nice practicability [1–3]. Hence, it is interesting and challenging to develop novel and effective enzyme mimetics. Recently, various enzyme mimetics have been reported and widely used in clinical diagnosis and biomedical analysis, including nanomaterials [4–7], Schiff-base complexes [8], cyclodextrin [9], hemin [10], and DNA complexes [11]. Among them, nanomaterials are becoming a novel efficient mimic peroxidase in catalyzing H_2O_2 -mediated reaction due to their intrinsic properties like natural enzymes in size, shape and surface charge [4–6]. Moreover, nanomaterials exhibit nice surface properties with larger specific surface areas, more surface activation centers, and controlled catalytic potentials, which can highly promote their peroxidase-like catalytic performances [5]. Thus, the field for seeking novel nanomaterials such as peroxidase mimetics has been rapidly developed since Fe_3O_4 magnetic nanoparticles were first found to present the intrinsic peroxidase-like activity like that of horseradish peroxidase (HRP) in 2007 [4]. Thereafter, many kinds of nanomaterials have been exploited as peroxidase mimetics, and have exhibited good peroxidase-like properties, such as magnetic nanomaterials ($CoFe_2O_4$ [12] and $FeVO_4$ [13]), carbon nanomaterials (carbon nanotubes [14], carbon dots [15], graphene oxides [16], and C_3N_4 [17]), noble metal nanomaterials (gold, silver and platinum) [18] and their alloys ($AgVO_3$ nanobelts [19], $FeSe-Pt@SiO_2$ nanospheres [20], Fe_3O_4-Pt nanocomposites [21], and Fe_3O_4-Au nanohybrids [22]), and other nanomaterials ($BiOI$ nanoflowers [23], $CeVO_4$ nanorods [24] and MoS_2 nanoflakes [25]). Despite this progress, there is still an urgent demand to pursue novel nanomaterials with highly-efficient and stable peroxidase-like activities to overcome their inherent disadvantages, including the loss of noble metals, environmental pollution, difficulty in separation, and recyclability.

Recently, special attention has been focused on graphene-like, two-dimensional (2D) nanomaterials owing to their 2D layer structure with high energy surfaces analogous to graphene [25–27]. As typical 2D nanomaterials, graphitic carbon nitride ($g-C_3N_4$) possesses a stacked 2D structure and appropriate band gap (2.7 eV) owing to the sp^2 hybridization of carbon and nitrogen, resulting in the formation of a stable and extended π -conjugated system [25–27]. And the unique graphite-like structure and tunable electronic structure of $g-C_3N_4$ lead to its large specific surface area, high thermal and chemical stability, and rapid electron transfer, accompanied by the advantage of being metal-free, abundant in natural resources, and economical, endowing $g-C_3N_4$ with extensive potential for use in new energy, sensor, and catalysis applications [25–27]. Currently, $g-C_3N_4$ materials have been reported as peroxidase mimetics [17], showing nice peroxidase-like activities and further extending their application areas in biotechnology. However, in view of the high recombination rate of photoinduced electron-hole pairs, the catalytic efficiency of pure $g-C_3N_4$ is greatly restricted [27]. Hence, various methods have been performed to further improve the catalytic activity. Among them, constructing a functionalized hybrid structure using $g-C_3N_4$ as the supporter by doping with other efficient catalysts is an especially effective way, which can apparently adjust the electronic structure and accelerate electron transport [28,29]. Up to now, lots of $g-C_3N_4$ -based composites have been designed and exploited to explore the synergistic enhancement effect, such as $Cu/g-C_3N_4$ [28], $MnSe-g-C_3N_4$ nanosheets [29], $Fe-g-C_3N_4$ [30], $Co-g-C_3N_4$ [31], $g-C_3N_4/BiFeO_3$ nanocomposites [32], and so on, all of which exhibited an improved peroxidase-like activity. Therefore, in-depth investigations are indeed of great demand for designing and fabricating novel $g-C_3N_4$ -based nanocomposites to further facilitate the peroxidase-like activity.

As one of the typical 2D transition metal dichalcogenides, MoS_2 materials show excellent catalytic activity and long-term stability, which has been widely used in the fields of electronic devices, battery materials, and catalysts [33,34]. In addition, when the size decreased to less than 10 nm, MoS_2 QDs will exhibit unique extra electrical/optical properties owing to the stronger quantum confinement and edge effects [35,36], further improving its catalytic performance. Moreover, MoS_2 with diverse nanostructures (nanoflakes [25] and nanoparticles [37]) and several MoS_2 -based hybrids [38–40] have been reported as enzyme mimetics recently. Thus, on account of the matching energy band structure and nice catalytic performance, MoS_2 QDs is becoming an ideal candidate for coupling with $g-C_3N_4$ to

facilitate the peroxidase-like ability by promoting the separation and transport of electron-hole pairs. However, to the best of our knowledge, the peroxidase-like activity of MoS₂ QDs-g-C₃N₄ hybrids has not been investigated until now, which deserves further and deeper exploration.

Herein, in view of the superiority of g-C₃N₄ and MoS₂ QDs, the MoS₂@CNNS nanocomposites with different morphologies and surface properties were successfully designed and prepared via a protonation-assisted ion exchange method, which were used as efficient artificial enzymes. With the assistance of H₂O₂, the MoS₂@CNNS nanocomposites could catalyze the oxidation of the peroxidase substrate TMB to generate a blue colored reaction. Thus, a simple, rapid, ultrasensitive, selective, and stable system for the colorimetric detection of H₂O₂ was developed (Scheme 1). In addition, the morphology, crystal structure, surface properties, catalytic kinetics and mechanism, reusability and selectivity of the MoS₂@CNNS nanocomposites were studied. The peroxidase-like catalytic activities of MoS₂@CNNS nanocomposites had been greatly enhanced after the incorporation between CNNS and MoS₂ QDs, which could be mainly attributed to the synergistic interaction, accompanied by the more negative charge and larger specific surface area. The MoS₂@CNNS nanocomposites could have promising and broad applications in catalysis, biotechnology, and clinical diagnostics.



Scheme 1. Schematic illustration of peroxidase-like catalytic reaction of MoS₂@CNNS nanocomposites.

2. Materials and Methods

2.1. Materials and Reagents

MoS₂ powder and 3,3',5,5'-Tetramethylbenzidine (TMB) were purchased from Sigma-Aldrich (Shanghai, China). Melamine (C₃H₆N₆), Na₂MoO₄·2H₂O, Tioacetamida (TAA, CH₃CSNH₂), 1-methyl-2-pyrrolidone (NMP, C₅H₉NO), HCl, H₂O₂ (3 wt %), ethanol, isopropanol alcohol (IPA), *p*-benzoquinone (BQ), FeCl₃·6H₂O, CuSO₄·5H₂O, KNO₃, NaClO, glucose (Glu), lactose (Lac), L-valine (L-Val), glycine (Gly), and other chemicals were all of analytical grade and were purchased from Sinopharm Chemical Reagent Co., Ltd. (Shanghai, China). Lircon antiseptic liquid was obtained from Shandong Lierkang Disinfection Technology Co., Ltd. (Dezhou, China). All aqueous solutions were prepared with Milli-Q water (Millipore, Boston, MA, USA).

2.2. Preparation of the Catalysts

The MoS₂@CNNS nanocomposites were prepared according to our previous report by an in-situ ion exchange method in a protonation process [36]. The bulk g-C₃N₄ was firstly prepared via a calcination process. Then g-C₃N₄ nanosheets (CNNS) were obtained by the ultrasonic exfoliation method using bulk g-C₃N₄ powder. After a protonation process in HCl (37%) and an ion exchange

process under a hydrothermal condition, the MoS₂@CNNS nanocomposites were finally obtained and denoted as MoS₂@CNNS(30) ('30' stands for the molar ratio of Na₂MoO₄·2H₂O/CNNS was 30:1).

In addition, other MoS₂@CNNS nanocomposites with different molar ratio were prepared as controls under the same conditions as those mentioned above, which were denoted as MoS₂@CNNS(15) and MoS₂@CNNS(45), respectively. Moreover, pure MoS₂ QDs were prepared as control via an ultrasonic exfoliation method [41]. In brief, 100 mg of MoS₂ powder was added into 10 mL of NMP and sonicated for 3.5 h. Then, the dispersion was kept stable overnight and centrifuged at 5500 r/min for 90 min. Finally, the MoS₂ QDs were obtained by collecting the top part of the dispersion.

2.3. Characterization

The crystal phase and structure of the as-prepared samples were analyzed by powder X-ray diffraction (XRD) measurements on a Germany Bruker D8 Advanced powder diffractometer using Cu K_α radiation ($\lambda = 0.15406$ nm). The morphology and microstructure of the as-prepared samples were observed by transmission electron microscopy (TEM), high resolution transmission electron microscopy (HRTEM), and selected area electron diffraction (SAED) (JEOL JEM-2100, Tokyo, Japan). Contents of S and Mo in MoS₂@CNNS nanocomposites were measured via an inductively coupled plasma emission spectrometer (ICP-AES, Varian725-ES, Palo Alto, CA, USA). The specific surface areas were determined by an automatic nitrogen adsorption specific surface and pore size distribution analyzer (NOVA 4000e, Quantachrome Instruments, Boynton Beach, FL, USA) at 77 K after a pretreatment at 473 K for 2 h. The zeta potential tests were determined on a zeta potential measuring instrument (Zetasizer Nano-ZS, Malvern Instruments Ltd., Malvern, UK), which was examined six times (each time being the average of 100 runs) at pH 4.0, and the mean values and standard deviations were calculated automatically based on Smoluchowski's equation.

2.4. Peroxidase-Like Activities and Steady-State Kinetic Assay

The catalytic oxidation experiments (a peroxidase substrate TMB with H₂O₂) were carried out at room temperature to comparably investigate the peroxidase-like activities of the as-prepared catalysts, including MoS₂ QDs, CNNS and MoS₂@CNNS nanocomposites. Typically, the tests were performed by adding 200 μ L of 600 μ g/mL catalysts into the reaction systems containing 500 μ L of 50.0 mM phosphate buffer solution (PBS, pH = 4.0), 100 μ L of 8.0 mM TMB, and 200 μ L of 10.0 mM H₂O₂. Then, the reaction systems were monitored in a time-scan mode at 652 nm by an UV-visible spectrophotometer (Shimadzu UV-2500, Kyoto, Japan) right after all of the components were added and mixed. The effect of MoS₂@CNNS(30) concentration (0–200 μ g/mL), H₂O₂ concentration (0–5.0 mM), pH (2.0–9.0), and temperature (10–50 °C) on the peroxidase-like activity of MoS₂@CNNS(30) were also tested by the same procedures mentioned above to probe the optimal reaction conditions (Supplementary Information Figure S2 and Figure S3).

The steady-state kinetic tests were performed in a time course mode at 652 nm by an UV-visible spectrophotometer under the optimal experimental conditions (25.0 mM PBS, pH = 4.0, 25 °C, 120 μ g/mL MoS₂@CNNS(30)) by varying the concentration of TMB at a fixed concentration of H₂O₂ or vice versa [4,42]. The Michaelis-Menten constant was measured using the Lineweaver-Burk double reciprocal plot according to the equation $1/v = (K_m/V_{max}) \times (1/[S]) + 1/V_{max}$ [4,42], where v is the initial reaction velocity, K_m is the Michaelis-Menten constant, V_{max} is the maximum reaction velocity, and $[S]$ is the concentration of substrate.

2.5. Analysis of Active Species

To explore the roles of active species played in the catalytic reaction, the active species trapping experiments were carried out. In brief, scavengers (10.0 mM IPA, a scavenger of \cdot OH; 10.0 mM BQ, a scavenger of \cdot O₂⁻) were added into the reaction systems respectively to remove the active species under the optimal experimental conditions [23,24,43]. Then, the absorbance and color change of the reaction system was recorded at 652 nm by an UV-visible spectrophotometer.

2.6. H₂O₂ Detection

A colorimetric detection system of H₂O₂ was set up based on the nice peroxidase-like performances of MoS₂@CNNS(30). The reaction system contained 100 μL of 8.0 mM TMB, 200 μL of 600 μg/mL MoS₂@CNNS(30), 200 μL of H₂O₂ with different concentrations (0–0.1 mM), and 500 μL of 50.0 mM PBS (pH = 4.0). Then, the absorbance change of the mixture was recorded on time-mode at 652 nm with an UV-visible spectrophotometer to obtain a standard curve.

In addition, the specificity and selectivity of MoS₂@CNNS(30)-based detection system were evaluated by adding some potential interfering substances into the reaction system under the same experimental conditions mentioned above, such as metal and non-metal ions (20.0 mM of Fe³⁺, Cu²⁺, NO₃⁻, and ClO⁻) and common organic compounds (20.0 mM of glucose (Glu), lactose (Lac), L-valine (L-Val), and glycine (Gly)). The practical detection assay of H₂O₂ based on MoS₂@CNNS(30) was performed by adding commercial antiseptic solution (containing about 0.79 M H₂O₂) into the reaction system instead of standard H₂O₂ with the other operations fixed. The antiseptic liquid was diluted 1000 times before the test.

2.7. Stability and Reusability of the Catalysts

The stability and reusability of MoS₂@CNNS(30) were studied by recycling the H₂O₂ detection assays 10 times under optimal experimental conditions. The reaction system was monitored at 652 nm by a UV-visible spectrophotometer for 10 min. After each cycle, the MoS₂@CNNS(30) samples were collected by centrifugation, washed with Milli-Q water and alcohol, dried at 60 °C for 30 min, and then reused in the next cycle. The crystal structure and morphology of MoS₂@CNNS(30) samples after 10 cycles were characterized by XRD and TEM as described above.

3. Results

3.1. Characterization of the Catalysts

The crystal phase, structure, and crystallinity of the as-prepared samples were determined by XRD. It can be seen in Figure 1a that two tiny diffraction peaks can be barely seen in the XRD pattern of MoS₂ QDs, which can be attributed to the (100) and (110) lattice planes of MoS₂, respectively. However, the two diffraction peaks were extremely weak, which implied that the MoS₂ QDs had poor crystallinity [36]. In addition, the CNNS samples show a strong peak at 27.29°, which can be attributed to the characteristic of the stacking peak of π-conjugated layers and indexed for the interlayer reflection of a graphite-like structure as the (002) peak [29,36,44], consistent with the literature value (JCPDS No. 87-1526). Moreover, the absence of a (100) peak and the presence of a sharp (002) peak further confirmed the layered structures of CNNS samples and the good crystallinity of CNNS. As for the MoS₂@CNNS composites (Figure 1b), all the characteristic diffraction peaks can be well indexed to the graphite-like structure of CNNS (JCPDS No. 87-1526) and hexagonal phase MoS₂ (JCPDS Card No. 37-1492), indicating that MoS₂ QDs were successfully formed on the surface of CNNS through the aid of ion-exchange process. Furthermore, with increasing the loading amount of MoS₂ QDs, the relative intensity of corresponding (100) and (110) diffraction peaks of MoS₂ strengthened gradually, while the characteristic peaks of MoS₂ were still relatively weak and broad in the composites owing to the size effect of quantum dots. There were no significant shifts of the characteristic diffraction peaks occurring in the MoS₂@CNNS composites, implying that MoS₂ QDs existed as a separate phase rather than being incorporated into the lattice of CNNS [36]. No impurity peaks were observed in the obtained samples, indicating the pure phase of the samples. Hence, these results indicated that the MoS₂@CNNS nanocomposites were successfully obtained through the synergistic effect of anion-exchange and hydrothermal process.

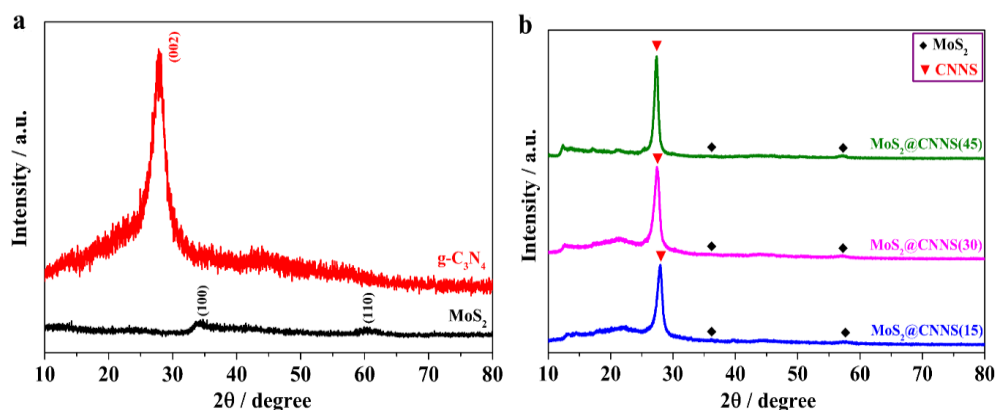


Figure 1. XRD patterns of MoS₂ QDs and g-C₃N₄ (a) and MoS₂@CNNS nanocomposites (b).

To obtain more detailed information about the morphologies and microstructures of the as-prepared catalysts, TEM and HRTEM characterizations were carried out. It can be seen in Figure 2a that the MoS₂ QDs showed a highly homogeneously monodispersed QDs nanostructures with the diameter of about 2–3 nm, indicating the successful preparation of MoS₂ QDs through the ultrasonic exfoliation method in NMP. Figure 2b presents a typical morphology of slabs with wrinkles of bulk g-C₃N₄, and after ultrasonic treatment for 16 h, the three-dimensional (3D) structure of bulk g-C₃N₄ was broken up into CNNS with 2D lamellar structure with the thickness of about 2.5 nm (Figure 2c). Thus, the as-prepared 2D CNNS nanosheets exhibited a thinner and exfoliated lamellar structure, which could provide a larger surface area and more reactive sites in the MoS₂@CNNS nanocomposites. Figure 2d–f shows the typical TEM images of MoS₂@CNNS nanocomposites. It can be seen that the MoS₂ QDs with the diameter of about 2.5–5.5 nm were uniformly distributed on the surface of CNNS nanosheets, and with increasing the amount of Na₂MoO₄·2H₂O in the ion exchange process, more and larger MoS₂ QDs were formed. No MoS₂ QDs were observed except for the surface of CNNS, indicating that the elaborate protonation effect in the ion exchange process led to the in-situ nucleation and growth of MoS₂ QDs on the surface of CNNS. And the large surface area of CNNS provided a nice reaction area, which effectively promoted the in-situ reaction process, resulting in the successful formation of MoS₂@CNNS nanocomposites. Moreover, the HRTEM image was examined to give further insight into the crystal structure of the MoS₂@CNNS(30) nanocomposites corresponding to the circled region in Figure 2e. It can be seen in Figure 2g that a lattice spacing of 0.65 nm was obviously shown in the CNNS, which is in accordance with the (002) lattice plane of tetragonal C₃N₄. In addition, the QDs displayed well-defined lattice fringes parallel to each other with the same interplanar spacing of 0.27 nm, which can be indexed to the (100) lattice plane of hexagonal-phase MoS₂. Meanwhile, several apparent diffraction rings were observed in the selected area electron diffraction (SAED) pattern of MoS₂@CNNS(30) (Figure 2h), which can be well indexed to the lattice planes of MoS₂ and g-C₃N₄, respectively, coinciding well with the XRD results. Therefore, these results indicated that a close-contact and well-defined MoS₂@CNNS nanostructure was formed via the planar in-situ growth of uniformly-dispersed MoS₂ QDs on the surface of CNNS during the protonation-assisted ion exchange process, which is a facile and controllable approach to obtain uniform and dispersive MoS₂ QDs on the surface of substrate.

In order to further probe the contents of S and Mo in MoS₂@CNNS nanocomposites, ICP-AES was examined. Quantitative analysis results showed the loading amount of MoS₂ QDs on the surface of CNNS is about 2.0, 5.7 and 5.7 wt % for MoS₂@CNNS(15), MoS₂@CNNS(30) and MoS₂@CNNS(45), respectively (Table S1). These results indicated that with increasing the amount of Na₂MoO₄·2H₂O in the ion exchange process, the loading capacity and protonated reactive site of CNNS was reaching saturation, which greatly restricted the formation of more MoS₂ QDs.

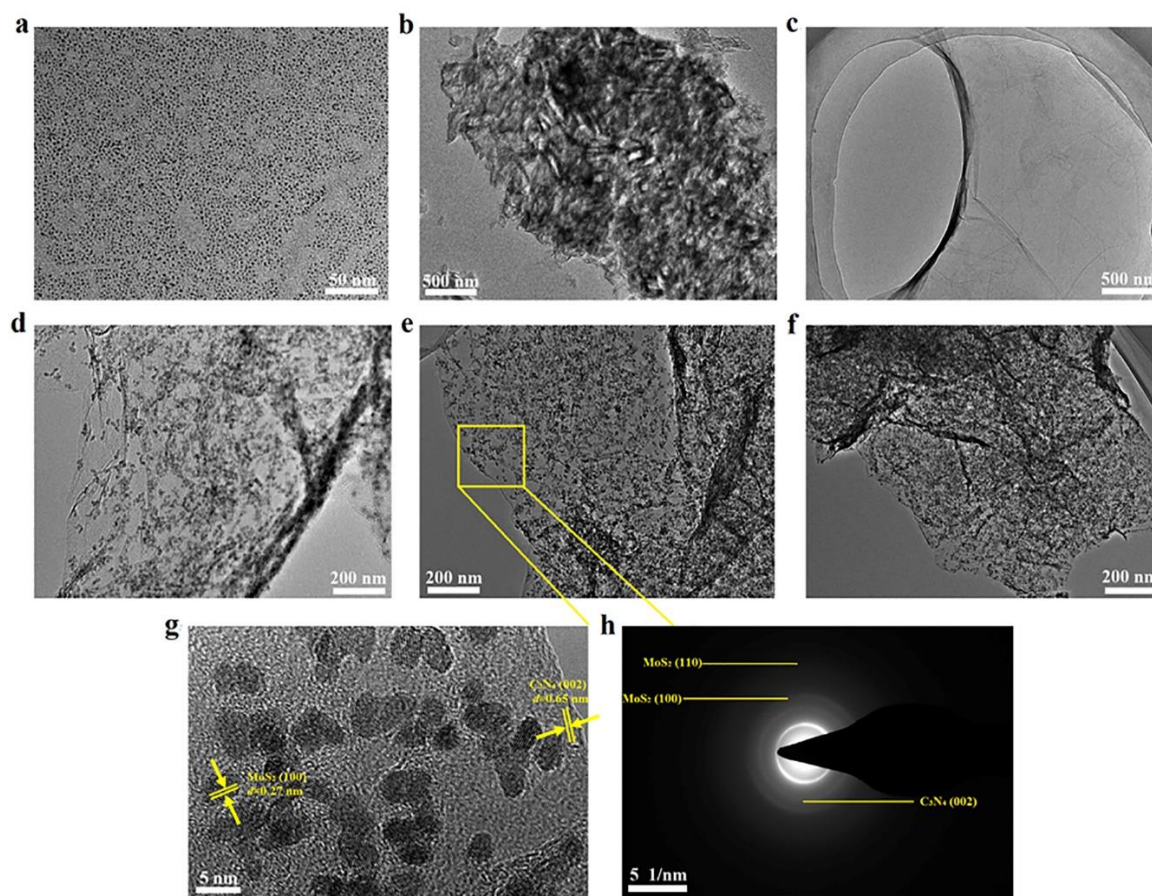


Figure 2. TEM images of MoS₂ QDs (a), bulk g-C₃N₄ (b), CNNS (c), MoS₂@CNNS(15) (d), MoS₂@CNNS(30) (e), and MoS₂@CNNS(45) (f); HRTEM image (g) and SAED pattern (h) of MoS₂@CNNS(30).

In addition, the Brunauer Emmett Teller (BET) specific surface area is a significant affecting factor for the catalytic abilities of catalysts, which was determined by the nitrogen adsorption method [23,24,45]. And the specific surface areas of MoS₂@CNNS(15), MoS₂@CNNS(30), MoS₂@CNNS(45), CNNS, and MoS₂ QDs were measured as 45.58, 75.93, 69.37, 29.85 and 16.13 m²/g, respectively. It can thus be seen that the MoS₂@CNNS(30) nanocomposites presented a larger specific surface area among the as-prepared catalysts (Figure S1a), though MoS₂@CNNS(45) loaded a little bit more MoS₂ QDs, while the agglomeration of the QDs could decrease the specific surface area. As is well known, a larger specific surface area will lead to more active sites, better adsorption performance, and faster electron transfer for catalysts, and will further improve the catalytic activities. Hence, MoS₂@CNNS(30) nanocomposites are expected to display enhanced peroxidase-like activity.

Furthermore, the zeta potentials of the MoS₂@CNNS nanocomposites were tested to explore their adsorption properties to molecules with different charges, which is also a significant indicator of the catalytic activities for catalysts. Thus, the zeta potentials of MoS₂@CNNS nanocomposites were determined as −30.48, −63.38, −53.66, −16.35 and −3.76 mV for MoS₂@CNNS(15), MoS₂@CNNS(30), MoS₂@CNNS(45), CNNS, and MoS₂ QDs, respectively (Figure S1b). The results indicated that different quantities of MoS₂ QDs loaded onto the surface of CNNS contributed to different surface charges of MoS₂@CNNS nanocomposites, which would further lead to different peroxidase-like activities. Therefore, based on the XRD, TEM, ICP-AES, BET, and zeta potential results mentioned above, it can be deduced that the MoS₂@CNNS nanocomposites prepared via the protonation-assisted ion exchange process showed different morphologies and structures due to the molar ratio

of $\text{Na}_2\text{MoO}_4 \cdot 2\text{H}_2\text{O}/\text{CNNS}$, leading to their different surface/interface properties and further contributing to the distinct peroxidase-like performance.

3.2. Peroxidase-Like Activities of $\text{MoS}_2@\text{CNNS}(30)$ Nanocomposites

To investigate the peroxidase-like activity of $\text{MoS}_2@\text{CNNS}(30)$ nanocomposites, the TMB catalytic oxidation experiments were conducted with or without H_2O_2 by the UV-visible absorption spectra in the range of 400–800 nm. It can be seen in Figure 3a that low absorption presented in the TMB + $\text{MoS}_2@\text{CNNS}(30)$, the H_2O_2 + TMB system, and the H_2O_2 + $\text{MoS}_2@\text{CNNS}(30)$ system, while the H_2O_2 + TMB + $\text{MoS}_2@\text{CNNS}(30)$ system exhibited an evident absorption peak at 652 nm, indicating that the $\text{MoS}_2@\text{CNNS}(30)$ nanocomposites could play a key role in catalyzing the oxidation of TMB in the presence of H_2O_2 . In addition, the significant color changes of different reaction systems were observed in Figure 3b, which coincided with the absorption spectra. It can be seen that the TMB + $\text{MoS}_2@\text{CNNS}(30)$ system, the H_2O_2 + TMB system, and the H_2O_2 + $\text{MoS}_2@\text{CNNS}(30)$ system were almost colorless. However, the H_2O_2 + TMB + $\text{MoS}_2@\text{CNNS}(30)$ system showed an apparent color variation, presenting a deep blue color, further demonstrating the excellent peroxidase-like properties of the $\text{MoS}_2@\text{CNNS}(30)$ nanocomposites.

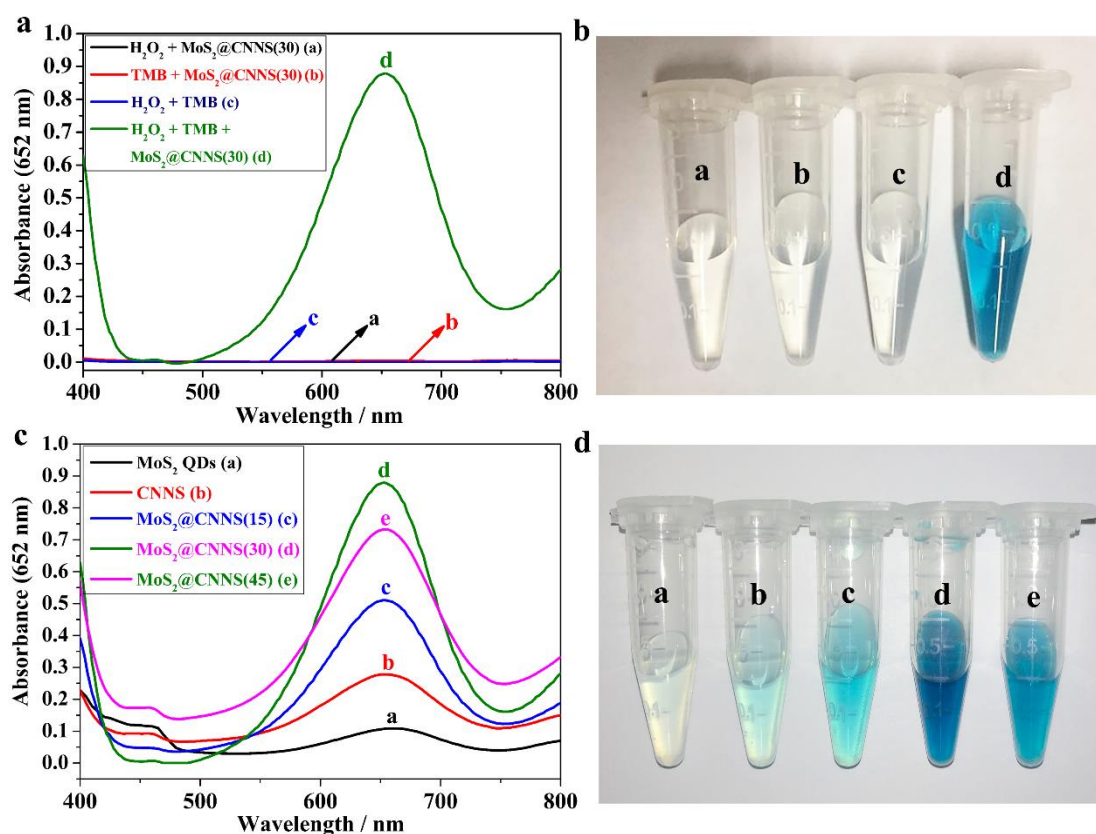


Figure 3. UV-visible absorption spectra (a) and color changes (b) of different reaction systems (a. H_2O_2 + $\text{MoS}_2@\text{CNNS}(30)$, b. TMB + $\text{MoS}_2@\text{CNNS}(30)$, c. H_2O_2 + TMB, and d. H_2O_2 + TMB + $\text{MoS}_2@\text{CNNS}(30)$); UV-visible absorption spectra (c) and color changes (d) in the presence of different $\text{MoS}_2@\text{CNNS}$ nanocomposites.

What's more, the peroxidase-like activities of other $\text{MoS}_2@\text{CNNS}$, pure MoS_2 QDs, and CNNS samples were studied and compared via the catalytic oxidation of TMB in the presence of H_2O_2 . It can be seen in Figure 3c that the $\text{MoS}_2@\text{CNNS}(30)$ -based assay system revealed the strongest absorption peak at 652 nm, followed by $\text{MoS}_2@\text{CNNS}(45)$, $\text{MoS}_2@\text{CNNS}(15)$, CNNS, and MoS_2 QDs, confirming the best peroxidase-like catalytic activity of $\text{MoS}_2@\text{CNNS}(30)$. The color variations of

different reaction systems also presented a similar result with the absorption spectra. As shown in Figure 3d, the MoS₂@CNNS(30)-based assay system showed the deepest blue color compared to that of other materials. Therefore, these results further indicated the enhanced peroxidase-like activities of the MoS₂@CNNS(30) nanocomposites compared to other MoS₂@CNNS nanocomposites, pure CNNS, and MoS₂ QDs. The more negative charge, larger specific surface area, and stable nanostructure of MoS₂@CNNS(30) mainly facilitated its superior and enhanced peroxidase-like performance, which could increase the binding affinity and absorption to TMB molecules, improve the electron transfer, accelerate the reaction rate, and further improve the peroxidase-like catalytic performance [29]. On the other hand, one can find that both CNNS and MoS₂ QDs showed a certain intrinsic peroxidase-like catalysis behavior toward TMB-H₂O₂ reaction, which could be attributed to the quantum effect and catalysis-active segments of MoS₂ QDs and CNNS. Thus, when MoS₂ QDs were loaded on CNNS by the in-situ growth process, the resulting MoS₂@CNNS(30) nanocomposites could display much higher peroxidase-like activities than pure CNNS and MoS₂ QDs on account of the synergistic effect of high conductivity and electron transfer capability for CNNS and highly-efficient intrinsic catalytic activity for MoS₂ QDs [29,36]. The bonding carbon network in CNNS could donate electrons to reduce H₂O₂ by accelerating the electron transfer from microcosmic point of view [29]. Furthermore, as a good supporter, CNNS could apparently improve the aqueous dispersion and stability of the nanocomposites. Thus, all of the favorable factors effectively improved the peroxidase-like performances of MoS₂@CNNS(30) nanocomposites. Hence, these results confirmed the enhanced peroxidase-like activities of the MoS₂@CNNS(30) nanocomposites, making it a potential highly-efficient colorimetric sensor for H₂O₂ detection.

3.3. Steady-State Kinetics Assay

For further insight into the peroxidase-like catalytic behavior of the MoS₂@CNNS(30) nanocomposites, the steady-state kinetic assays were carried out with H₂O₂ and TMB as substrates. The kinetic data were collected by changing the concentration of one substrate while keeping the other substrate concentration constant [4,42]. Thus, the typical Michaelis-Menten curves were recorded by varying the concentration of TMB or H₂O₂ while keeping the other one constant, as shown in Figure 4a,b. The steady-state kinetic reaction parameters were calculated on the basis of the Lineweaver-Burk double reciprocal plot (Figure 4c,d) according to the Michaelis-Menten equation: $1/v = (K_m/V_{max}) \times (1/[S]) + 1/V_{max}$, where v is the initial velocity, K_m is the Michaelis-Menten constant, V_{max} represents the maximal reaction velocity, and $[S]$ signifies the concentration of the substrate [4,29,38,42,46,47], which were listed in Table S2. It is well known that K_m is an important indicator of the binding affinity of enzyme to the substrates, and that it affects the reaction rate; a smaller value of K_m generally means a stronger affinity between the enzyme and the substrate [4,29,38,42,46,47]. As listed in Table S2, the K_m value of MoS₂@CNNS(30) with TMB was obviously lower than that of the natural enzyme HRP, implying that MoS₂@CNNS(30) had a stronger binding affinity to TMB than HRP, which might be attributed to the CNNS carriers with strong adsorption to TMB [4,29,38,42]. In addition, the V_{max} of MoS₂@CNNS(30) with TMB was more than two times larger than that of HRP, indicating a favorable tendency of a higher reaction rate, which could be the result of the presence of tiny MoS₂ QDs loaded on the surface of CNNS, as well as the rapid electron transfer capability of CNNS itself [29,36,38]. The K_m value of MoS₂@CNNS(30) with H₂O₂ was higher than that of HRP, suggesting a lower binding affinity between MoS₂@CNNS(30) and H₂O₂ than that of HRP. Furthermore, the typical Michaelis-Menten behavior towards TMB and H₂O₂ with various concentrations in the peroxidase-like catalytic reaction were measured, respectively. And the double-reciprocal plots (Figure 4c,d) of initial velocity against one substrate concentration showed the characteristic parallel lines, indicating a typical ping-pong mechanism of the peroxidase-like catalytic reaction [4,23,24,29,38,42,46,47]. Hence, these results inferred that MoS₂@CNNS(30) bound and reacted with the first substrate and then released the first product before reacting with the second substrate, which is similar to that of HRP [1–4,42,48].

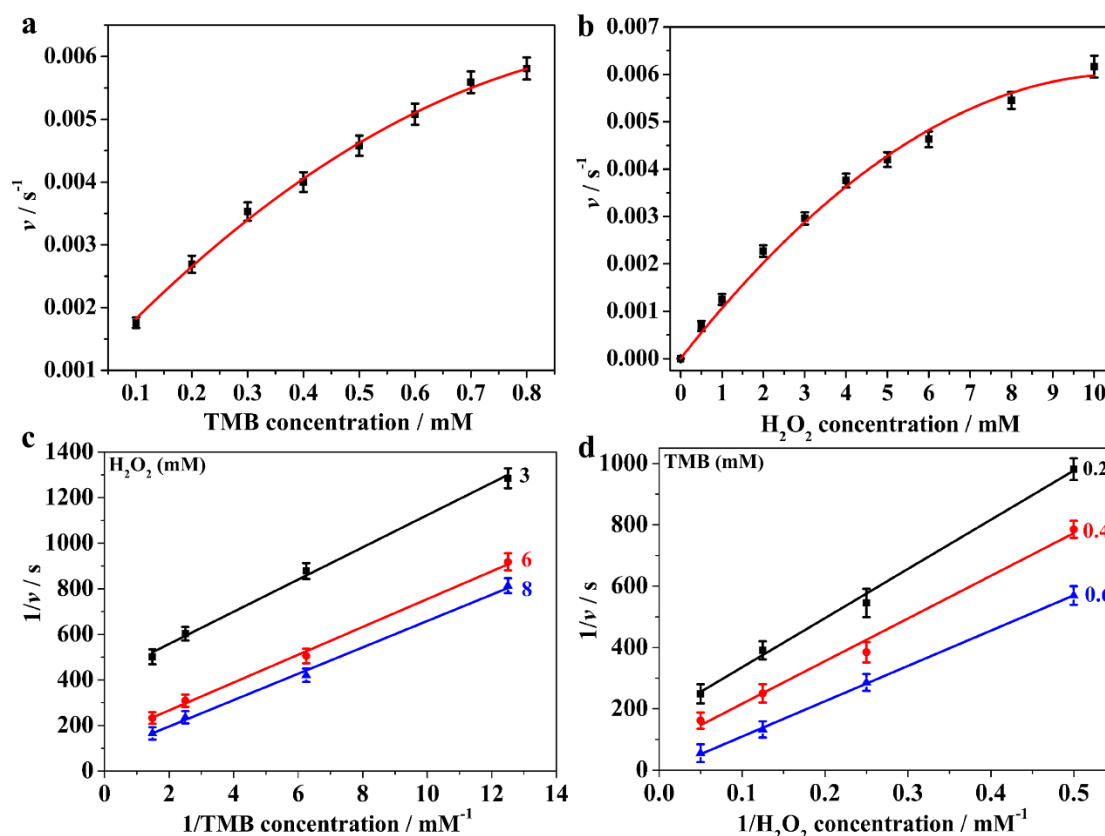


Figure 4. Steady-state kinetic analysis. The reaction velocity (v) was measured using 120 $\mu\text{g}/\text{mL}$ of $\text{MoS}_2@\text{CNNS}(30)$ in 25.0 mM PBS (pH = 4.0) at room temperature. The TMB concentration was varied while the concentration of H_2O_2 was 2.0 mM (a), the H_2O_2 concentration was varied while the concentration of TMB was 0.8 mM (b), and the double-reciprocal plots with a fixed concentration of one substrate relative to varying the concentration of the other substrate (c) and (d).

3.4. Active Species Analysis and Peroxidase-Like Catalytic Mechanism Study

It is reported that the reaction system contained H_2O_2 , which would easily produce some active radicals such as $\cdot\text{OH}$ and $\cdot\text{O}_2^-$ that could play significant roles in catalytic reaction [23,24,49,50]. Hence, in order to explore the peroxidase-like catalytic mechanism of $\text{MoS}_2@\text{CNNS}(30)$ nanocomposites, active species trapping experiments were carried out by adding different scavengers (IPA as $\cdot\text{OH}$ scavengers and BQ as $\cdot\text{O}_2^-$ scavengers) into the reaction systems under other fixed experimental conditions. It can be seen in Figure 5 that an evident decrease in absorption and color fading of the reaction system was seen with the addition of BQ, while little change in absorption and color was observed after adding IPA. These results indicated that the $\text{MoS}_2@\text{CNNS}(30)$ nanocomposites could catalytically activate H_2O_2 to generate $\cdot\text{O}_2^-$ radicals in the peroxidase-like catalytic reaction, which subsequently play major roles in oxidizing TMB to produce a TMB oxide with a blue color.

On the basis of the above experimental results and some previous literature [1–4,23,24,28–32,37–40], the peroxidase-like catalytic mechanism of $\text{MoS}_2@\text{CNNS}(30)$ nanocomposites was proposed, and is illustrated in Scheme 1. It can be seen that the negatively-charged $\text{MoS}_2@\text{CNNS}(30)$ nanocomposites could act as the peroxidase mimics, facilitating the electron transfer between TMB and H_2O_2 in the catalytic oxidation reaction. During the reaction process, many positively-charged TMB molecules would be absorbed onto the surface of $\text{MoS}_2@\text{CNNS}(30)$ nanocomposites owing to the large specific surface area, acting as the chromogenic electron donors. Then, the TMB molecules would donate the lone-pair electrons from the amino groups to the surface of $\text{MoS}_2@\text{CNNS}(30)$ nanocomposites, enhancing the density and mobility of electrons on the surface of $\text{MoS}_2@\text{CNNS}(30)$, then promoting

the electron transfer from MoS₂@CNNS(30) to H₂O₂, and further accelerating the TMB catalytic oxidation reaction rate [4,23,24,28–32,37–40]. Subsequently, the oxidized intermediate ·O₂[−] radicals generated in the reaction between MoS₂@CNNS(30) and H₂O₂ via one electron transfer would react with TMB molecules to generate a TMB oxide, leading to the color change of the system from colorless to blue [4,23,24,28–32,37–40]. The corresponding chemical equation was: 2H₂O₂ + TMB $\xrightarrow{\text{catalysts}}$ 2H₂O + O₂ + oxTMB. Hence, in light of the excellent peroxidase-like catalytic activity, MoS₂@CNNS(30) nanocomposites exhibited a promising application prospect in medical diagnostics and environmental assay.

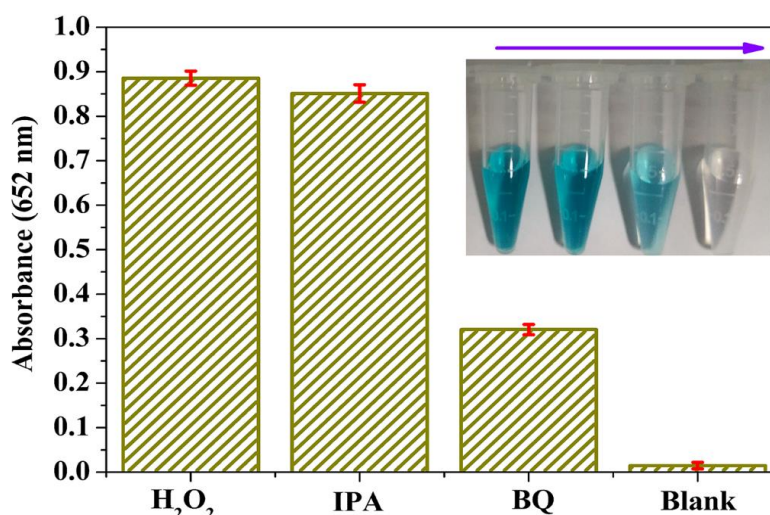


Figure 5. Time-dependent absorbance of reaction solutions at 652 nm in the absence or presence of scavengers (10 mM of IPA and BQ) containing 25.0 mM PBS (pH = 4.0), 2.0 mM H₂O₂, 0.8 mM TMB, and 120 µg/mL MoS₂@CNNS(30) at room temperature. Inset: related color changes.

3.5. Detection of H₂O₂ by MoS₂@CNNS(30)-Based Assay System

On the basis of the aforementioned intrinsic and enhanced peroxidase-like catalytic activity of MoS₂@CNNS(30), a simple, rapid and ultrasensitive colorimetric method for the visual detection of H₂O₂ was developed. As the absorbance of oxidized TMB was in proportion to the H₂O₂ concentration, it was a simple approach to determine H₂O₂ at 652 nm only by the naked eye, or by using an UV-visible spectrometer. Figure 6a shows the time-course dependent absorbance changes at 652 nm of the oxidized TMB in the presence of H₂O₂ with different concentrations. It can be seen that the reaction rate increased by increasing the concentration of H₂O₂ from 0.002 mM to 0.10 mM. Moreover, it can be seen in Figure 6b that the typical H₂O₂ concentration-response curve displayed a linear response in the range of 2.0 µM to 50.0 µM, and the linear fitting equation is $A_{652\text{nm}} = 1.63 \times 10^{-3} + 0.748C$ (mM), with a correlation coefficient of 0.9956. Hence, the detection limit of H₂O₂ was estimated to be 0.02 µM. In addition, as shown in the inset of Figure 6b, the color variation for H₂O₂ response as low as 1.0 µM was also apparently observed by the naked eye, which offered a convenient approach to detect H₂O₂ even at low concentrations. Furthermore, compared to some other previously-reported nanomaterials with peroxidase-like activities [17,25,29,30,37,39,42,46,51] (Table S3), MoS₂@CNNS(30) nanocomposites revealed a reasonable linear range and a lower detection limit for H₂O₂ detection, further confirming their superior peroxidase-like catalytic activity and sensitivity. Therefore, these results indicated that the visual biosensing platform based on MoS₂@CNNS(30) was a simple, rapid, and convenient method for H₂O₂ detection with ultrasensitive response.

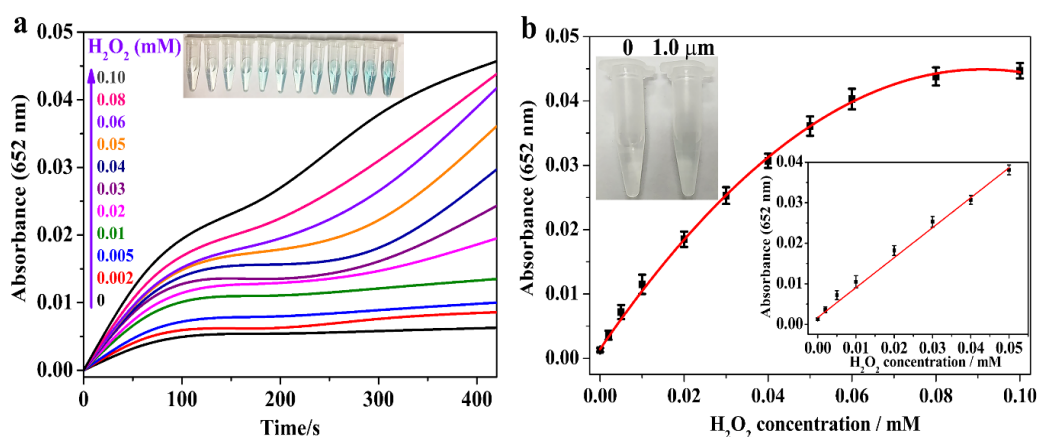


Figure 6. Time-dependent absorbance changes at 652 nm in the presence of different concentrations of H₂O₂ in 25.0 mM PBS (pH = 4.0) with 120 μg/mL MoS₂@CNNS(30) and 0.8 mM TMB at room temperature (a) and a dose-response curve for H₂O₂ detection (b). Inset: related color changes and the linear calibration plot of H₂O₂.

3.6. Selectivity and Applicability of MoS₂@CNNS(30)-Based Assay System

To estimate the selectivity of MoS₂@CNNS(30)-TMB-H₂O₂ detection system, some other substances, such as Fe³⁺, Cu²⁺, NO₃⁻, ClO⁻, Glu, Lac, L-Val, and Gly, with the concentration of 20.0 mM were added into the reaction system respectively as the potential interferents instead of H₂O₂. In addition, a commercial antiseptic liquid (diluted 1000 times) was used to check the practical applicability and accuracy of the H₂O₂ detection system in a real sample (RS). It can be seen in Figure 7 that no evident absorbance at 652 nm and color change were observed, though the concentrations of these interferents were 10 times higher than that of standard H₂O₂ (2.0 mM), indicating a nice selectivity of the detection system. Moreover, the diluted commercial antiseptic liquid presented an obvious absorbance and light blue color, and the concentration of H₂O₂ in the commercial antiseptic liquid could be calculated to be about 0.77 M based on the calibration curve shown in Figure 6b, which was close to the actual concentration of the commercial antiseptic liquid (0.79 M). Therefore, these results exhibited the favorable applicability in complicated conditions of the MoS₂@CNNS(30)-based H₂O₂ detection system, which favored the practical and rapid determination of H₂O₂ in various environments.

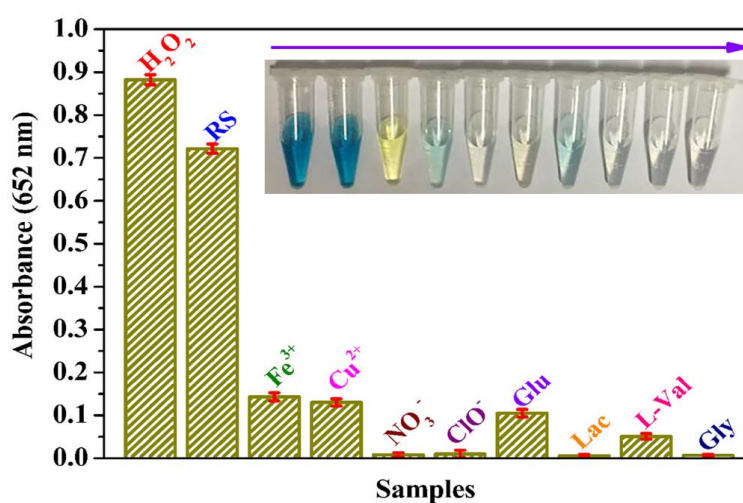


Figure 7. Reveal sample (antiseptic liquid was diluted 1000 times) and selectivity analysis with interfering substances (20.0 mM of Fe³⁺, Cu²⁺, NO₃⁻, ClO⁻, Glu, Lac, L-Val, and Gly) of MoS₂@CNNS(30)-based assay system by monitoring the absorbance at 652 nm. Inset: related color changes.

3.7. Stability and Reusability of MoS₂@CNNS(30)-Based Assay System

In order to study the stability and reusability of MoS₂@CNNS(30)-based H₂O₂ detection system, the peroxidase-like experiments were conducted by repeating the reaction for ten successive cycles. After each cycle, the MoS₂@CNNS(30) samples were collected, washed several times with Milli-Q water and ethanol, and dried, and then reused in the next cycle. Every cycle lasted for 10 min. It can be seen in Figure 8a,b that there was no significant change of the reaction system absorbance at 652 nm during the recycling tests, accompanied by no color variations of the reaction system observed in the recycling tests, showing the excellent reusability and stable peroxidase-like performance of the MoS₂@CNNS(30)-based H₂O₂ detection system. The relative standard deviation (RSD) of the absorbance values was only 1.72%, which further confirmed the nice reproducibility, stability, and reusability of the MoS₂@CNNS(30)-based assay system even for 10 cycles. Moreover, XRD and TEM were used to further analyze the crystal structure and morphology of MoS₂@CNNS(30) after ten successive cycles. It can be seen in Figure 8c that the XRD pattern of MoS₂@CNNS(30) after ten successive cycles displayed no apparent change in both peak intensity and position, implying the stable crystal structure of MoS₂@CNNS(30) samples kept in the recycling tests. In addition, no significant morphology variation was observed in the TEM image of MoS₂@CNNS(30) samples after ten successive cycles (Figure 8d), though a little impurity appeared on the surface of CNNS, exhibiting the good stability in crystal structure and morphology. Hence, good stability, reusability, reproducibility and precision of the MoS₂@CNNS(30)-based assay system suggested that the peroxidase-like colorimetric method might be used to analyze H₂O₂ in real water samples, which also favored long-term use.

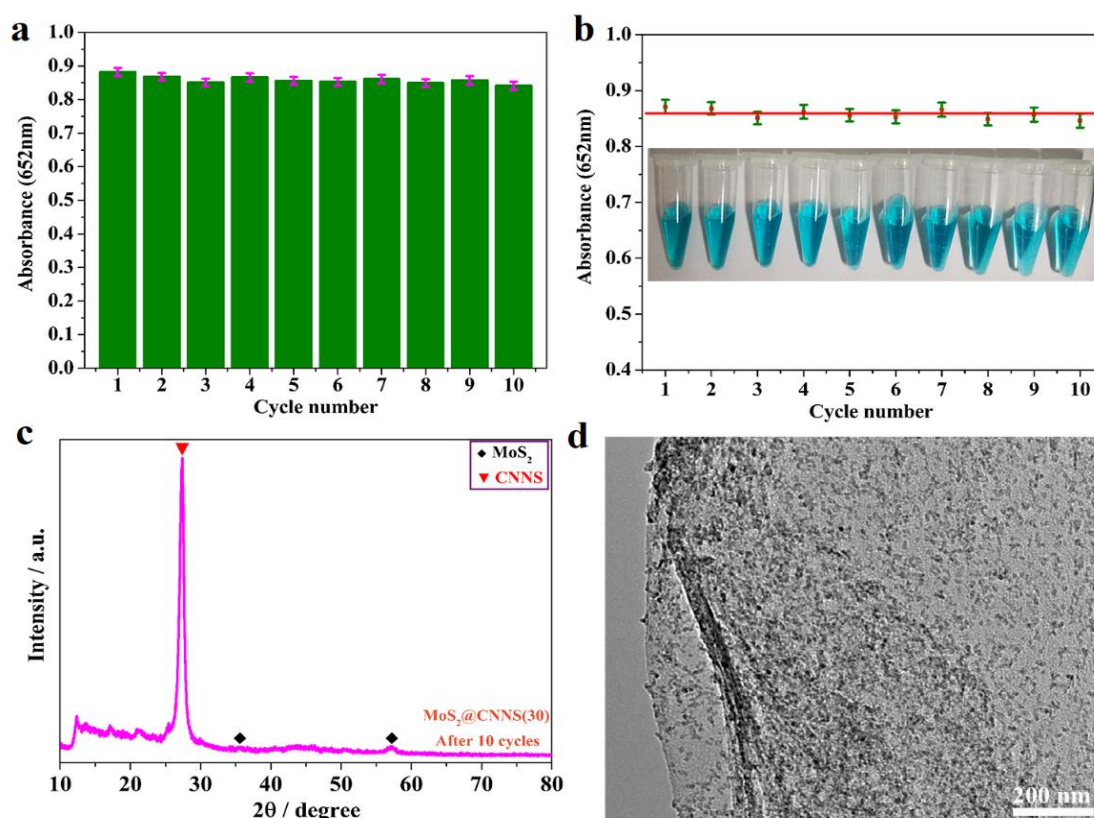


Figure 8. Stability and reusability experiments of MoS₂@CNNS(30)-based assay system containing 120 μg/mL MoS₂@CNNS(30), 25.0 mM PBS (pH = 4.0), 2.0 mM H₂O₂, and 0.8 mM TMB (a), (b); XRD pattern (c) and TEM image (d) of MoS₂@CNNS(30) after 10 cycles. Inset: related color changes in 10 cycles.

4. Conclusions

In conclusion, the MoS₂@CNNS nanocomposites were successfully synthesized via a protonation-assisted ion exchange method, which were demonstrated to display an enhanced intrinsic peroxidase-like activity. The in-situ growth of MoS₂ QDs on the surface of ultrathin CNNS formed a stable nanostructure, facilitating the synergetic effects of high conductivity and electron-transfer capability for CNNS and intrinsic catalytic activity for MoS₂ QDs, and thus, greatly improving the peroxidase-like performance of the nanocomposites. In addition, the MoS₂@CNNS nanocomposites revealed different morphologies, surface properties, and peroxidase-like activities, owing to the different amount of MoS₂ QDs loading on the surface of CNNS. The MoS₂@CNNS(30) nanocomposites showed the best peroxidase-like ability among the composites, which could be attributed to their more negative potential and larger specific surface area. In the presence of H₂O₂ and the peroxidase substrate TMB, MoS₂@CNNS(30) could induce a typical blue color reaction, thus providing a colorimetric assay for H₂O₂. The catalytic activity was strongly dependent on the catalyst concentration, H₂O₂ concentration, pH, and temperature. Moreover, the kinetic and active species trapping experiments indicated that the catalytic reaction followed a ping-pong mechanism, and the ·O₂⁻ radicals played a pivotal role in the peroxidase-like catalytic reaction. Based on the excellent peroxidase-like catalytic performance of MoS₂@CNNS(30) nanocomposites, a simple, rapid, and ultrasensitive platform for colorimetric detection of H₂O₂ was developed, which exhibited a nice selectivity, reusability, long-term stability, and practicability, making it a potential biosensing material for the practical applications in H₂O₂ detection and biomedical analysis. Furthermore, this work offers some new insights and targeted directions for novel enzymatic mimics with enhanced catalytic activity.

Supplementary Materials: The following are available online at <http://www.mdpi.com/2079-4991/8/12/976/s1>, Figure S1: Adsorption/desorption isotherms of MoS₂@CNNS(30) (a) and zeta potentials of the MoS₂@CNNS nanocomposites dispersed in ultrapure water (pH = 4.0) (b), Figure S2: Time-dependent absorbance at 652 nm and color changes of 0.8 mM TMB reaction solutions in the absence or presence of different concentrations of MoS₂@CNNS(30) (a) and H₂O₂ (b) in 25.0 mM PBS (pH = 4.0) at room temperature. Inset: related color variations, Figure S3: Dependency of peroxidase-like activity of MoS₂@CNNS(30) on pH (a) and temperature (b) and color changes. Experiments were conducted by using 120 µg/mL of MoS₂@CNNS(30) in 25.0 mM PBS with 2.0 mM H₂O₂ and 0.8 mM TMB as substrates; Inset: related color variations, Table S1: MoS₂ loading amount in MoS₂/CNNS samples determined by ICP-AES, Table S2: Comparison of K_m and V_{max} between MoS₂@CNNS(30) and HRP for H₂O₂ and TMB, Table S3: Comparison of peroxidase-like activity in the linear range and detection limit of H₂O₂ between MoS₂@CNNS(30) and other peroxidase mimics.

Author Contributions: Conceptualization, P.J. and Y.H.H.; methodology, P.J. and Y.H.H.; software, X.X.H.; validation, P.J. and C.J.S.; formal analysis, Y.H.H. and M.W.; investigation, P.J., Y.H.H. and M.W.; resources, P.J. and C.J.S.; data curation, Y.H.H. and M.W.; writing—original draft preparation, P.J. and Y.H.H.; writing—review and editing, P.J.; visualization, F.H.J.; supervision, C.W. and C.J.S.; project administration, P.J. and C.J.S.; funding acquisition, P.J. and C.J.S.

Funding: This research was supported by National Natural Science Foundation of China (51702328), Key Lab of Marine Bioactive Substance and Modern Analytical Technique, SOA (MBSMAT-2016-05), Natural Science Foundation of Shandong Province, China (ZR2017BD002), China Postdoctoral Science Foundation Funded Project (2017M622179 and 2018T110681), CAS “Light of West China” Program, Open Fund of Laboratory for Marine Ecology and Environmental Science, Pilot National Laboratory for Marine Science and Technology (Qingdao) (LMEES201802), Open Foundation of Pilot National Laboratory for Marine Science and Technology (Qingdao) (QNLM2016ORP0410), and The Aoshan Scientific and Technological Innovation Project Financially Supported by Pilot National Laboratory for Marine Science and Technology (Qingdao) (2016ASKJ14). C.J. Sun would also like to thank support from Taishan Scholar and the Ministry of Human Resources and Social Security of China.

Conflicts of Interest: The authors declare no conflict of interest.

References

1. Song, Y.J.; Wei, W.L.; Qu, X.G. Colorimetric biosensing using smart materials. *Adv. Mater.* **2011**, *23*, 4215–4236. [[CrossRef](#)] [[PubMed](#)]
2. Wei, H.; Wang, E.K. Nanomaterials with enzyme-like characteristics (nanozymes): Next-generation artificial enzymes. *Chem. Soc. Rev.* **2013**, *42*, 6060–6093. [[CrossRef](#)] [[PubMed](#)]

3. Wang, Q.Q.; Wei, H.; Zhang, Z.Q.; Wang, E.K.; Dong, S.J. Nanozyme: An emerging alternative to natural enzyme for biosensing and immunoassay. *TrAC-Trend. Anal. Chem.* **2018**, *105*, 218–224. [[CrossRef](#)]
4. Gao, L.; Zhuang, J.; Nie, L.; Zhang, J.; Zhang, Y.; Gu, N.; Wang, T.; Feng, J.; Yang, D.; Perrett, S.; Yan, X. Intrinsic peroxidase-like activity of ferromagnetic nanoparticles. *Nat. Nanotechnol.* **2007**, *2*, 577–583. [[CrossRef](#)] [[PubMed](#)]
5. Tian, R.; Sun, J.H.; Qi, Y.F.; Zhang, B.Y.; Guo, S.L.; Zhao, M.M. Influence of VO₂ nanoparticle morphology on the colorimetric assay of H₂O₂ and glucose. *Nanomaterials* **2017**, *7*, 347. [[CrossRef](#)] [[PubMed](#)]
6. Zheng, H.Q.; Liu, C.Y.; Zeng, X.Y.; Chen, J.; Lv, J.; Lin, R.G.; Cao, R.; Lin, Z.J.; Su, J.W. MOF-808: A metal-organic framework with intrinsic peroxidase-like catalytic activity at neutral pH for colorimetric biosensing. *Inorg. Chem.* **2018**, *57*, 9096–9104. [[CrossRef](#)] [[PubMed](#)]
7. Zhou, R.; Guzman, M.I. Photocatalytic reduction of fumarate to succinate on ZnS mineral surfaces. *J. Phys. Chem. C* **2016**, *120*, 7349–7357. [[CrossRef](#)]
8. Vázquez-Fernández, M.Á.; Bermejo, M.R.; Fernández-García, M.I.; González-Riopedre, G.; Rodríguez-Doutón, M.J.; Maneiro, M. Influence of the geometry around the manganese ion on the peroxidase and catalase activities of Mn(III)=Schiff base complexes. *J. Inorg. Biochem.* **2011**, *105*, 1538–1547. [[CrossRef](#)] [[PubMed](#)]
9. Yang, Z.; Ji, H. 2-Hydroxypropyl-β-cyclodextrin polymer as a mimetic enzyme for mediated synthesis of benzaldehyde in water. *ACS Sustain. Chem. Eng.* **2013**, *1*, 1172–1179. [[CrossRef](#)]
10. Wang, Q.G.; Yang, Z.M.; Zhang, X.Q.; Xiao, X.D.; Chang, C.K.; Xu, B. A supramolecular-hydrogel-encapsulated hemin as an artificial enzyme to mimic peroxidase. *Angew. Chem. Int. Ed.* **2007**, *46*, 4285–4289. [[CrossRef](#)] [[PubMed](#)]
11. Tan, B.; Zhao, H.M.; Wu, W.H.; Liu, X.; Zhang, Y.B.; Quan, X. Fe₃O₄-AuNPs anchored 2D metal-organic framework nanosheets with DNA regulated switchable peroxidase-like activity. *Nanoscale* **2017**, *9*, 18699–18710. [[CrossRef](#)] [[PubMed](#)]
12. Wu, L.H.; Wan, G.P.; Hu, N.; He, Z.Y.; Shi, S.H.; Suo, Y.R.; Wang, K.; Xu, X.F.; Tang, Y.L.; Wang, G.Z. Synthesis of porous CoFe₂O₄ and its application as a peroxidase mimetic for colorimetric detection of H₂O₂ and organic pollutant degradation. *Nanomaterials* **2017**, *7*, 451. [[CrossRef](#)] [[PubMed](#)]
13. Yu, Y.Z.; Ju, P.; Zhang, D.; Han, X.X.; Yin, X.F.; Zheng, L.; Sun, C.J. Peroxidase-like activity of FeVO₄ nanobelts and its analytical application for optical detection of hydrogen peroxide. *Sensor. Actuator. B Chem.* **2016**, *233*, 162–172. [[CrossRef](#)]
14. Wang, H.; Li, P.H.; Yu, D.Q.; Zhang, Y.; Wang, Z.Z.; Liu, C.Q.; Qiu, H.; Liu, Z.; Ren, J.S.; Qu, X.G. Unraveling the enzymatic activity of oxygenated carbon nanotubes and their application in the treatment of bacterial infections. *Nano Lett.* **2018**, *6*, 3344–3351. [[CrossRef](#)] [[PubMed](#)]
15. Singh, V.K.; Yadav, P.K.; Chandra, S.; Bano, D.; Talat, M.; Hasan, S.H. Peroxidase mimetic activity of fluorescent NS-carbon quantum dots and their application in colorimetric detection of H₂O₂ and glutathione in human blood serum. *J. Mater. Chem. B* **2018**, *6*, 5256–5268. [[CrossRef](#)]
16. Song, Y.; Qu, K.; Zhao, C.; Ren, J.; Qu, X. Graphene oxide: intrinsic peroxidase catalytic activity and its application to glucose detection. *Adv. Mater.* **2010**, *22*, 2206–2210. [[CrossRef](#)] [[PubMed](#)]
17. Lin, T.R.; Zhong, L.S.; Wang, J.; Guo, L.Q.; Wu, H.Y.; Guo, Q.Q.; Fu, F.F.; Chen, G.N. Graphite-like carbon nitrides as peroxidase mimetics and their applications to glucose detection. *Biosens. Bioelectron.* **2014**, *59*, 89–93. [[CrossRef](#)] [[PubMed](#)]
18. Guo, S.J.; Wang, E.K. Noble metal nanomaterials: Controllable synthesis and application in fuel cells and analytical sensors. *Nano Today* **2011**, *6*, 240–264. [[CrossRef](#)]
19. Xiang, Z.B.; Wang, Y.; Ju, P.; Zhang, D. Optical determination of hydrogen peroxide by exploiting the peroxidase-like activity of AgVO₃ nanobelts. *Microchim. Acta* **2016**, *183*, 457–463. [[CrossRef](#)]
20. Qiao, F.M.; Wang, Z.; Xu, K.; Ai, S.Y. Double enzymatic cascade reactions within FeSe-Pt@SiO₂ nanospheres: synthesis and application toward colorimetric biosensing of H₂O₂ and glucose. *Analyst* **2015**, *140*, 6684–6691. [[CrossRef](#)] [[PubMed](#)]
21. Kim, M.S.; Kweon, S.H.; Cho, S.Y.; An, S.S.A.; Kim, M.I.; Doh, J.S.; Lee, J.W. Pt-decorated magnetic nanozymes for facile and sensitive point-of-care bioassay. *ACS Appl. Mater. Interfaces* **2017**, *9*, 35133–35140. [[CrossRef](#)] [[PubMed](#)]

22. Cho, S.Y.; Shin, H.Y.; Kim, M.I. Nanohybrids consisting of magnetic nanoparticles and gold nanoclusters as effective peroxidase mimics and their application for colorimetric detection of glucose. *Biointerphases* **2017**, *12*, 01A401. [[CrossRef](#)] [[PubMed](#)]
23. Ju, P.; Xiang, Y.H.; Xiang, Z.B.; Wang, M.; Zhao, Y.; Zhang, D.; Yu, J.Q.; Han, X.X. BiOI hierarchical nanoflowers as novel robust peroxidase mimetics for colorimetric detection of H₂O₂. *RSC Adv.* **2016**, *6*, 17483–17493. [[CrossRef](#)]
24. Ju, P.; Yu, Y.Z.; Wang, M.; Zhao, Y.; Zhang, D.; Sun, C.J.; Han, X.X. Synthesis of EDTA-assisted CeVO₄ nanorods as robust peroxidase mimics towards colorimetric detection of H₂O₂. *J. Mater. Chem. B* **2016**, *4*, 6316–6325. [[CrossRef](#)]
25. Yu, J.; Ma, D.Q.; Mei, L.Q.; Gao, Q.; Yin, W.Y.; Zhang, X.; Yan, L.; Gu, Z.J.; Ma, X.Y.; Zhao, Y.L. Peroxidase-like activity of MoS₂ nanoflakes with different modifications and their application for H₂O₂ and glucose detection. *J. Mater. Chem. B* **2018**, *6*, 487–498. [[CrossRef](#)]
26. Fan, H.; Wang, N.; Tian, Y.J.; Ai, S.Y.; Zhan, J.H. Acetic acid induced synthesis of laminated activated carbon nitride nanostructures. *Carbon* **2016**, *107*, 747–753. [[CrossRef](#)]
27. Li, Y.; Jin, R.; Xing, Y.; Li, J.; Song, S.; Liu, X.; Li, M.; Jin, R. Macroscopic foam-like holey ultrathin g-C₃N₄ nanosheets for drastic improvement of visible-light photocatalytic activity. *Adv. Energy Mater.* **2016**, *24*, 1601273. [[CrossRef](#)]
28. Wang, N.; Han, Z.W.; Fan, H.; Ai, S.Y. Copper nanoparticles modified graphitic carbon nitride nanosheets as a peroxidase mimetic for glucose detection. *RSC Adv.* **2015**, *5*, 91302–91307. [[CrossRef](#)]
29. Qiao, F.M.; Qi, Q.Q.; Wang, Z.Z.; Xu, K.; Ai, S.Y. MnSe-loaded g-C₃N₄ nanocomposite with synergistic peroxidase-like catalysis: Synthesis and application toward colorimetric biosensing of H₂O₂ and glucose. *Sensor. Actuator. B Chem.* **2016**, *229*, 379–386. [[CrossRef](#)]
30. Tian, J.Q.; Liu, Q.; Asiri, A.M.; Qusti, A.H.; Al-Youbi, A.O.; Sun, X.P. Ultrathin graphitic carbon nitride nanosheets: a novel peroxidase mimetic, Fe doping-mediated catalytic performance enhancement and application to rapid, highly sensitive optical detection of glucose. *Nanoscale* **2013**, *5*, 11604–11609. [[CrossRef](#)] [[PubMed](#)]
31. Mu, J.S.; Li, J.; Zhao, X.; Yang, E.C.; Zhao, X.J. Cobalt-doped graphitic carbon nitride with enhanced peroxidase-like activity for wastewater treatment. *RSC Adv.* **2016**, *6*, 35568–35576. [[CrossRef](#)]
32. Ouyang, H.; Tu, X.M.; Fu, Z.F.; Wang, W.W.; Fu, S.F.; Zhu, C.Z.; Du, D.; Lin, Y.H. Colorimetric and chemiluminescent dual-readout immunochromatographic assay for detection of pesticide residues utilizing g-C₃N₄/BiFeO₃ nanocomposites. *Biosens. Bioelectron.* **2018**, *106*, 43–49. [[CrossRef](#)] [[PubMed](#)]
33. Chhowalla, M.; Shin, H.S.; Eda, G.; Li, L.J.; Loh, K.P.; Zhang, H. The chemistry of two-dimensional layered transition metal dichalcogenide nanosheets. *Nat. Chem.* **2013**, *5*, 263–275. [[CrossRef](#)] [[PubMed](#)]
34. Huang, Y.X.; Guo, J.H.; Kang, Y.J.; Ai, Y.; Li, C.M. Two dimensional atomically thin MoS₂ nanosheets and their sensing applications. *Nanoscale* **2015**, *7*, 19358–19376. [[CrossRef](#)] [[PubMed](#)]
35. Wang, X.J.; Wu, Q.; Jiang, K.L.; Wang, C.X.; Zhang, C. One-step synthesis of water-soluble and highly fluorescent MoS₂ quantum dots for detection of hydrogen peroxide and glucose. *Sensor. Actuator. B Chem.* **2017**, *252*, 183–190. [[CrossRef](#)]
36. Wang, M.; Ju, P.; Zhao, Y.; Li, J.J.; Han, X.X.; Hao, Z.M. In situ ion exchange synthesis of MoS₂/g-C₃N₄ heterojunction for highly efficient hydrogen production. *New J. Chem.* **2018**, *42*, 910–917. [[CrossRef](#)]
37. Zhao, K.; Gu, W.; Zheng, S.S.; Zhang, C.L.; Xian, Y.Z. SDS-MoS₂ nanoparticles as highly-efficient peroxidase mimetics for colorimetric detection of H₂O₂ and glucose. *Talanta* **2015**, *141*, 47–52. [[CrossRef](#)] [[PubMed](#)]
38. Peng, J.; Weng, J. Enhanced peroxidase-like activity of MoS₂/graphene oxide hybrid with light irradiation for glucose detection. *Biosens. Bioelectron.* **2017**, *89*, 652–658. [[CrossRef](#)] [[PubMed](#)]
39. Zhang, Y.; Zhou, Z.F.; Wen, F.F.; Tan, J.; Peng, T.; Luo, B.Q.; Wang, H.G.; Yin, S.X. A flower-like MoS₂-decorated MgFe₂O₄ nanocomposite: Mimicking peroxidase and colorimetric detection of H₂O₂ and glucose. *Sensor. Actuator. B Chem.* **2018**, *275*, 155–162. [[CrossRef](#)]
40. Vinita; Nirala, N.R.; Prakash, R. One step synthesis of AuNPs@MoS₂-QDs composite as a robust peroxidase-mimetic for instant unaided eye detection of glucose in serum, saliva and tear. *Sensor. Actuator. B Chem.* **2018**, *263*, 109–119. [[CrossRef](#)]
41. Gopalakrishnan, D.; Damien, D.; Shaijumon, M.M. MoS₂ quantum dot-interspersed exfoliated MoS₂ nanosheets. *ACS Nano* **2014**, *8*, 5297–5303. [[CrossRef](#)] [[PubMed](#)]

42. Wei, H.; Wang, E.K. Fe₃O₄ magnetic nanoparticles as peroxidase mimetics and their applications in H₂O₂ and glucose detection. *Anal. Chem.* **2008**, *80*, 2250–2254. [[CrossRef](#)] [[PubMed](#)]
43. Ye, L.; Chen, J.; Tian, L.; Liu, J.; Peng, T.; Deng, K.; Zan, L. BiOI thin film via chemical vapor transport: photocatalytic activity, durability, selectivity and mechanism. *Appl. Catal. B Environ.* **2013**, *130–131*, 1–7. [[CrossRef](#)]
44. Zhang, Y.; Thomas, A.; Antonietti, M.; Wang, X. Activation of carbon nitride solids by protonation: Morphology changes, enhanced ionic conductivity, and photoconduction experiments. *J. Am. Chem. Soc.* **2009**, *131*, 50–51. [[CrossRef](#)] [[PubMed](#)]
45. Ju, P.; Wang, Y.; Sun, Y.; Zhang, D. Controllable one-pot synthesis of a nest-like Bi₂WO₆/BiVO₄ composite with enhanced photocatalytic antifouling performance under visible light irradiation. *Dalton Trans.* **2016**, *45*, 4588–4602. [[CrossRef](#)] [[PubMed](#)]
46. Chen, L.J.; Sun, B.; Wang, X.; Qiao, F.M.; Ai, S.Y. 2D ultrathin nanosheets of Co-Al layered double hydroxides prepared in L-asparagine solution enhanced peroxidase-like activity and colorimetric detection of glucose. *J. Mater. Chem. B* **2013**, *1*, 2268–2274. [[CrossRef](#)]
47. Qiao, F.M.; Chen, L.J.; Li, X.; Li, L.; Ai, S.Y. Peroxidase-like activity of manganese selenide nanoparticles and its analytical application for visual detection of hydrogen peroxide and glucose. *Sensor. Actuator. B Chem.* **2014**, *193*, 255–262. [[CrossRef](#)]
48. Porter, D.J.; Bright, H.J. The mechanism of oxidation of nitroalkanes by horseradish peroxidase. *J. Biol. Chem.* **1983**, *258*, 9913–9924. [[PubMed](#)]
49. Li, L.; Ai, L.; Zhang, C.; Jiang, J. Hierarchical {001}-faceted BiOBr microspheres as a novel biomimetic catalyst dark catalysis towards colorimetric biosensing and pollutant degradation. *Nanoscale* **2014**, *6*, 4627–4634. [[CrossRef](#)] [[PubMed](#)]
50. Wang, B.; Ju, P.; Zhang, D.; Han, X.X.; Zheng, L.; Yin, X.F.; Sun, C.J. Colorimetric detection of H₂O₂ using flower-like Fe₂(MoO₄)₃ microparticles as a peroxidase mimic. *Microchim. Acta* **2016**, *183*, 3025–3033. [[CrossRef](#)]
51. Chen, Q.; Chen, J.; Gao, C.J.; Zhang, M.L.; Chen, J.Y.; Qiu, H.D. Hemin-functionalized WS₂ nanosheets as highly active peroxidase mimetics for label-free colorimetric detection of H₂O₂ and glucose. *Analyst* **2015**, *140*, 2857–2863. [[CrossRef](#)] [[PubMed](#)]



© 2018 by the authors. Licensee MDPI, Basel, Switzerland. This article is an open access article distributed under the terms and conditions of the Creative Commons Attribution (CC BY) license (<http://creativecommons.org/licenses/by/4.0/>).